Digital, ultra-sensitive, end-point protein measurements with large dynamic range via Brownian trapping with drift

Shencheng Ge,‡ Weishan Liu,‡ Travis Schlappi, and Rustem F. Ismagilov*

Division of Chemistry and Chemical Engineering, California Institute of Technology, 1200 East California Boulevard, Pasadena, California 91125, United States

*Rustem F. Ismagilov, rustem.admin@caltech.edu
‡ These authors contributed equally.

Supporting information

Contents

S1. Theoretical description and analysis

Drift dominates the transport of analytes along a channel when the ratio of advection rate to diffusion rate is much greater than 1. The Péclet number characterizes this balance and is defined in the longitudinal direction as follows:

$$Pe_x = \frac{advection\ rate\ in\ x}{diffusion\ rate\ in\ x} = \frac{U/L}{D/L^2} = \frac{UL}{D} \qquad \text{Eq. S1}$$

In our experiment, the target analyte (protein) had a diffusion coefficient $D \sim 10^{-11}$ m^2/s, drift velocity $U \sim 10^{-5}$ m/s, and was flown past capture regions of length $L \sim 10^{-3}$ m, resulting in $Pe_x \sim 10^3$. Thus, longitudinal transport of an analyte molecule and its distance traveled as a function of time, $x(t)$, can be formulated to ignore diffusion effects and depends only on drift velocity: $x(t) \approx Ut$. Replacing $t \approx x/U$ in eq 1 converts the exponential decay over time into an exponential decay over space.

At the same time, flow should be slow enough that diffusion of the protein from the top to the bottom of the channel (H) is comparable relative to flow over one capture region. This ensures that analyte molecules aren't advected away before they have a chance to diffuse down to the capture beads. Again, the Péclet number formulates this comparison:

Eq. S2 $$Pe_z = \frac{advection\ rate\ in\ x}{diffusion\ rate\ in\ z} = \frac{U/L}{D/H^2}$$

In our experimental setup, $H = 50$ μm, resulting in $Pe_z \sim 2.5$.

Finally, for trapping to be effective and give rise to an exponential decay in space, the capture rate of analyte molecules onto the beads must be comparable to the transport rate away from the beads, as shown by the Damköhler number:

Eq. S3 $$Da = \frac{capture\ rate}{transport\ rate\ in\ x} = \frac{k_{on}[Ab]}{U/L}.$$

In our experimental setup, $k_{on} \sim 10^5$ M^{-1} s^{-1}, [Ab] $\sim 10^{-7}$ M, resulting in $Da \sim 1$.

Origin of the exponential decay in space

Exponential decay in space is reasonable because if capture efficiency in each region is constant, then connecting the regions in series will result in an exponential relationship between analyte molecules captured and region number.

Replacing $t = n \cdot \Delta t$ in eq 1, Eq. S4 represents the number of free analyte molecules in solution that survive up until the exit of region n ($n = 1,2,3 \ldots$), where Δt is the residence time over each region and C_0 is the initial amount of analytes.

Eq. S4 $$N_{free}(n) = C_0 e^{-\lambda n \Delta t}$$

Because the amount of captured molecules is simply the free molecules exiting the region subtracted from the free molecules entering the region, the capture efficiency can be calculated according to Eq. S5.

Eq. S5 $$\beta = \frac{\text{captured molecules in region } n}{\text{surviving molecules entering region } n} = \frac{C_0 e^{-\lambda(n-1)\Delta t} - C_0 e^{-\lambda n \Delta t}}{C_0 e^{-\lambda(n-1)\Delta t}} = 1 - e^{-\lambda \Delta t}$$

Because λ and Δt are both constant for this assay, the capture efficiency is constant in each region.

If the capture efficiency is constant in each region and the regions are connected together in series, one would expect an exponential decay for the free analytes in solution because they are reduced by a factor of β after each region. As long as there is an excess of capture antibodies, the capture process will only depend on the amount of free analytes in solution; thus, we also expect to see an exponential decay in captured analytes. In fact, solving Eq. S5 for the amount of captured analyte molecules in region n directly reveals this exponential relationship between captured analyte molecules ($N_{captured}$) and region number n.

Eq. S6 $$N_{captured}(n) = \beta C_0 e^{-\lambda(n-1)\Delta t}$$

S2. Materials

The superparamagnetic beads for enzyme measurement were Agilent LodeStar 2.7 Streptavidin (Agilent Technologies, Santa Clara, CA). The magnetic beads for TNF-α assays were Agilent LodeStar 2.7 Carboxyl (Agilent Technologies), covalently attached to the antibody by standard coupling chemistry. β-galactosidase from *Escherichia coli* (G3153, Sigma-Aldrich, St. Louis, MO) was biotinylated using the Chromalink biotinylation reagent and diluted in Starting Block T20 PBS (Thermo Scientific, Waltham, MA). Monoclonal anti-TNF-α antibody, recombinant TNF-α calibrator, and detection anti-TNF-α antibody were purchased from R&D Systems (Minneapolis, MN). The Streptavidin-β-galactosidase (SβG) conjugate and the enzyme substrate RGP were purchased from Life Technologies (Grand Island, NY). Pooled human serum was purchased from ValleyBiomedical (Winchester, VA). Bovine serum was purchased from Thermo Scientific (Waltham, MA). Fluorocarbon oils FC40 and FC3283 were obtained from 3M (St. Paul, MN). RfOEG (triethyleneglycol mono[1*H*,1*H*-perfluorooctyl]ether) was synthesized in the lab.

S3. Device fabrication

Sodalime and borofloat glass plates coated with Cr and photoresist (Telic company, Valencia, CA) were used to fabricate the device. Standard photolithographic methods were used to transfer the designed pattern, including the microwells and channels, onto the glass plates. The photomask was designed using Autocad and then printed on a transparent film (CAD/Art Services, Bandon, OR) or a Cr mask (Photo sciences, Torrance, CA) (Figure S1). A PDMS/glass adapter was used to connect the tubing to the device.

To fabricate the channels in the top plate of the device, we used a wet-etching method with hydrofluoric acid. Briefly, the back and side of the plate were taped to protect the bare glass from HF etching. Then the glass plates were immersed in HF etching solution at 40° C with continuous shaking. Photoresist/chrome served as the etching mask. All channels were etched to a depth of 50 µm. Typical etching rate under these conditions was 1.3 µm/min. After etching, plates were rinsed thoroughly with water to remove residual HF and blown dry with nitrogen.

Remaining photoresist and the chromium layer were removed by acetone and chrome etchant. Through holes were drilled at both ends of the channels and then the plate was thoroughly cleaned with piranha solution. Finally, the plate was air plasma treated for 100 s and subjected to gas-phase silanization using trichlorosilane (Tridecafluoro-1,1,2,2 –tetrahydrooctyl; Gelest Inc., Morrisville, PA) . Briefly, the vacuum in a glass desiccator was pumped down to 0.4 Torr at room temperature to facilitate the vaporization of fluorosilane, and then the chamber was closed for 1 h. Next, the plate was baked at 95° C overnight and rinsed by FC3283 to remove unbound silane. The plate was further baked for at least 30 min to complete the fluorosilanization procedure.

To fabricate microwells in the bottom half of the device for single-bead confinement, we used borofloat glass plates and a fluorine-based dry etching method with C4F8-based plasma. Briefly, the photoresist was removed from the glass plate following the photolithography step using acetone. The remaining Cr layer served as the dry-etching mask. The glass plate was mounted on a 6-in carrier wafer using thermogrease fomblin and subject to C4F8-based plasma etching (plasmalab 100, oxford instrument) under the following conditions: chamber pressure 10 mT, C4F8 flow rate 40 sccm, and ICP power 3000w. Typical etching rate under these conditions was 0.2–0.3 μm/min. Uniform single-bead loading per microwell is important for downstream digital readout and data interpretation using Poisson statistics. To improve etching uniformity across the plate, a two-step etching protocol was adopted. At the end of the first half of the etching step, the plate was removed from the chamber and subjected to a sonication-assisted wash to remove non-volatile residuals, such as sodium fluoride. Then the plate was rinsed by isopropanol and blown dry using nitrogen. The second half the etching step was performed with the plate rotated 180^{o} to increase etching uniformity.

A hydrophilic surface chemistry in the microwell is also important for successful bead loading, as hydrophobic wells fail to load beads. We chose to functionalize the microwell surface with PEG-silane both to render it hydrophilic and prevent non-specific protein adsorption. To fabricate PEGlated microwells on a hydrophobic surface, the dry-etched plate was first briefly etched with diluted HF in a sonication batch to regenerate the glass surface in the etched microwells. Then, the microwells were PEG-silanized. Briefly, 150 μL silane were dissolved in 100 mL toluene and then 80 μL HCl was added in a dropwise manner while the mixture was sonicated. The mixture was further sonicated for 10 min before use. The plate was immersed in this mixture and subjected to brief sonication to ensure wetting of the microwells. The plate was incubated at room temperature on a shaker for 1 h and washed sequentially by toluene and ethanol. Next, the plate was baked at 150° C for 30 min to finish the PEG silanization procedure. To protect the PEG chemistry in the etched microwells from downstream fluorosilanization, sacrificial resist was used to preserve the surface chemistry. The plate was spin-coated with a negative photoresist NR9-3000PY (Futurrex, Franklin, NJ) and baked. Then the plate was flipped and exposed to UV light using the Cr as an embedded mask. The photoresist was developed according to manufacturer's protocol. Next, the chrome layer was removed using chrome etchant. The plate was thoroughly rinsed by water and baked at 95° C for 30 min to dry. The plate was then air plasma treated and fluorosilanized using the protocol outlined above. Finally, the sacrificial photoresist was removed in hot DMSO (110° C, 10 min). The surface outside of the microwells functionalized with fluorinated silane is fluorophilic. This combination of hydrophilic and fluorophilic surface chemistry allows the microwells to be easily

compartmentalized for downstream digital readout by simply flowing fluorocarbon oils over the microwells.

To fabricate the PDMS/glass adapter, access holes were first drilled on a sodalime glass plate to match the inlet ports on the top half the device. A PDMS slab with matching access holes was then plasma-bonded to the glass plate. The complete adapter was plasma treated for 100 sec and fluorosilanzed following the procedure outlined above.

S4. Device operation and bead loading

The bottom half of the device was briefly sonicated in water to pre-wet the microwells. A wet cleanroom wipe was used to cover the regions of microwells. Then 100 μL of FC40 containing 0.4 mg/ml fluoro-surfactant RfOEG was applied to the plate along the cloth edge and the top half of the device was assembled. The wipe was gently pulled out from the gap and the additional FC40 was injected into the channels using manual pipettes. At this stage, the device is ready for bead loading.

Capture reagent-coated magnetic beads were stored in Starting Block PBS solution (TPBS) at 4° C. Prior to use, the beads were concentrated to 75 mg/ml in the same buffer and then 2-3 μL of the bead slurry was injected to the channel. Next, the device was held on the edge of a magnet so that the channel axis aligned with the magnet edge and the beads in the channel were pulled uniformly toward the channel side. While held on the magnet, the top glass plate was gently slipped away from the magnet and the beads were physically scraped against the magnetic pulling force. As a result, the beads were actively pulled into the well while the unloaded beads were removed from the surface. By using concentrated bead slurry and repeating the loading procedure, both high loading efficiency and uniformity in bead loading across the chip were obtained. Typical loading efficiency was >90%. The unloaded beads were collected, washed, and stored in TPBS for future use. Next, the device was manually aligned under a stereoscope so that the channels on the top plate aligned with the microwell features on the bottom. A PDMS/glass adapter was then used to connect Teflon tubing to the device inlets. The tubing contained the following solution sequence: FC40, 0.5 μL air, 2 μL FC40 and then 5 μL washing buffer (PBS with 0.05 % Tween-20). The solution sequence was pumped through the channel at a rate of 0.5ul/min to remove any loose beads. The microwells were finally resealed by FC40 and the device was stored on ice until use.

S5. Digital measurements of enzyme

Test solutions of biotinylated β-galactosidase were prepared by diluting in TPBS with 1 mM $MgCl_2$. The solutions of 3 μL are either (i) directly pipetted into the device and incubated for an hour; or (ii) gently aspirated into Teflon tubings and then delivered to the channels at 0.05 μL/min for 1 h, controlled by a syringe pump equipped with a multi-syringe rack. The device is then washed with 30 μL PBS with 0.05 % Tween-20 per channel. The device then is loaded with 100 mM RGP in PBS with 0.05 % Tween-20 and 1 mM $MgCl_2$, and digitized by flowing FC40 into the channels. The device was imaged after 15 minutes.

S6. Digital measurements of TNF-α

Standard ELISA procedure was followed to perform the on-chip digital immunoassay for TNF-α. Syringe pump and Teflon tubing preloaded with washing buffer and other reagent solution were

used to deliver the solution to the device. In addition, the assay was performed on a magnet to minimize bead loss.

Specifically, the calibrator sample were prepared in 25% bovine serum to 75% TPBS buffer. 25% pooled human serum sample was similarly prepared to measure the endogenous concentration of TNF-α. The antibody and β-galactosidase -streptavidin conjugate was diluted in TPBS. The washing buffers were 1x and 5x PBS containing 0.1% Tween-20 (1x PBST and 5x PBST). The solutions was preloaded into Teflon tubing and delivered to the 10 channels on the device simultaneously using a syringe pump equipped with a multi-syringe rack. The flow rate was 2 μL/min except at 0.1 μL/min for the sample plug. Throughout the assay, as multiple air-aqueous, air-oil and aqueous-oil interfaces migrated through the bead-loaded regions, the device was kept on a magnet to minimize bead loss. Solution sequence was stopped during incubation with detection antibody and enzyme conjugate and then resumed subsequently. The second (b) and third (c) solution sequences were pumped through the device from the opposite direction of the first solution sequence (a) to avoid potential cross-contamination of target analytes between regions. Details of the solution sequences were as follows (also see Fig. S3):
a. FC40, 0.5 μL air, 2 μL FC40, 2 μL 5x PBST, 0.5 μL air, 4 μL 5x PBST, 0.5 μL air, 2 μL 1x PBST, 0.5 μL air, and 8 μL serum sample.
b. FC40, 0.5 μL air, 2 μL FC40, 3 μL 5x PBST, 0.5 μL air, 3 μL 5x PBST, 0.5 μL air, 4 μL biotinylated detection antibody, 0.5 μL air, 4 μL 1x PBST.
c. FC40, 0.5 μL air, 2 μL FC40, 2 μL enzyme substrate, 0.5 μL air, 3 μL 1x PBST, 0.5 μL air, 5 μL 5x PBST (total 5 repeats), 4 μL streptavidin-galactosidase conjugate, 0.5 μL 1x PBST. All aqueous solutions were supplemented with 1 mM $MgCl_2$ to enhance the enzyme activity of β-galactosidase.

The total assay time takes ~ 6 h. Specifically, it takes ~0.5 h for bead loading, ~2 h for sample delivery for a volume of 8 μL, 1 h for incubation with a detection antibody, 0.5 h for incubation with streptavidin-galactosidase, ~0.5 h for washing, and ~1.5 h for incubation with substrate and subsequent imaging.

S7. Image acquisition and analysis

Fluorescence images were acquired in TexasRed and GFP channels on an inverted microscope equipped with a 0.63x camera adapter and a digital CCD camera using the autofocus function to enhance quality. Positive bead count and total bead count were analyzed based on threshold fluorescence intensity and morphological criteria. The image acquisition, processing and analysis were all performed using MetaMorph software (Molecular Devices, Sunnyvale, CA).

Specifically, the acquired images were digitally processed and analyzed using the following sequence in Metamorph: (a) subtract the uniform background arising from the dark current of the camera; (b) flatten the field of view to remove the bias in fluorescent intensity resulting from non-uniform illumination; (c) apply “No Neighbors” function in Metamorph to reduce the haze effect and improve contrast.

Next, the selection and quantification of positive beads were automatically performed using the Metamorph function of “threshold image” and “integrated morphometry analysis” based on the

following criteria: (a) Fluorescence intensity > 500 (Figure S5A); (b) "Area" range for inclusion: 2-50 pixels; (c) "Shape factor" range for inclusion: 0.9-1. Finally, the correct selection of positive beads was confirmed visually.

S8. Achieving a given dynamic range with fewer wells in digital assay with drift relative to a standard digital assay.

The Brownian trapping with drift format achieves a larger dynamic range with fewer wells than a standard digital format. This can potentially be useful in single cell analysis, and in multiplexed assays, where one wants each cell to use as few wells as possible in order to fit them all onto a chip. As an example, consider the theoretical calculation of dynamic ranges for a standard digital assay with 5000 wells compared to a digital assay with drift as described in this manuscript, but only containing 150 wells. The volume of sample analyzed is 5 μL and each well in both formats has a volume of 1 nL. Labeling efficiencies and background effects are ignored as this is a simplified model intended to compare the dynamic ranges, not predict actual outcomes.

Standard digital assay

LDL is the lower detection limit and is defined as the concentration which would have a 95% chance of generating a least one positive well and equals the concentration calculated from three positive wells [1]. To calculate the concentration from three positive wells, one uses Eq. 2 from Reference [1], which is derived from the Poisson distribution.

Eq. S7 $$LDL = -\frac{\ln\left(\frac{w-3}{w}\right)}{v}$$

For $w = 5000$ wells and a well volume $v = 1$ nL, $LDL = 0.6$ molecules/μL.

ULQ is the upper limit of quantification and is defined as the concentration which would have a 95% chance of generating at least one negative well and equals the concentration calculated on the basis of three negative wells [1].

Eq. S8 $$ULQ = -\frac{\ln\left(\frac{3}{w}\right)}{v}$$

For $w = 5000$ wells and a well volume $v = 1$ nL, $UQL = 7.42 \cdot 10^3$ molecules/μL. Thus, the dynamic range, ULQ/LDL, is $10^{4.09}$.

Digital assay with drift

The dynamic range of a digital assay with drift depends on how many regions there are, the capture efficiency of each region (β), and the number of wells in each region. Consider a microfluidic chip with 15 regions, 10 wells in each region, and a capture efficiency of 25%. The LDL for the drift assay can be calculated by asking what concentration one must start with in order to have three positive wells in the whole device. At the completion of the assay, the total amount of captured analyte molecules is simply the analyte molecules escaping region 15 (calculated with Eq. S4) subtracted from the initial amount, C_0.

Eq. S9 $$N_{captured} = C_0 - C_0 e^{-15\lambda \Delta t}$$

Setting Eq. S9 equal to Eq. S7 with $w = 150$ and $v = 1$ nL yields $C_0 = LDL = 20.5$molecules/μL.

The ULQ for the drift assay can be calculated by asking what concentration one must start with in order to have three negative wells in the final region (the preceding regions will all be saturated). The amount of captured analyte molecules in the 15th region is found from Eq. S6.

Eq. S10 $$N_{captured}(15) = \beta C_0 e^{-\lambda \Delta t(15-1)}$$

Setting Eq. S10 equal to Eq. S8 with $w = 10$ and $v = 1$ nL yields $C_0 = UQL = 2.70 \cdot 10^5$ molecules/μL. Thus, the dynamic range is $10^{4.12}$, which is comparable to the dynamic range of the standard digital assay, but with only 150 wells instead of 5000.

S9. Author contributions

W.L., S.G., and R.F.I. designed the SlipChip experiments. W.L., S.G. performed experiments and data analysis. T.S., W.L., S.G. performed theoretical analysis. W.L., S.G., T.S. and R.F.I. wrote the paper.
S.G. performed the dry-etching.
S.G. and W.L. fabricated devices.
W.L. performed the measurements for Fig. 3.
S.G. performed the measurements for Fig. 4.
W.L. and T.S. performed the COMSOL simulation for plots in Figure S6.

S10. Reference

[1] Jason E. Kreutz, Todd Munson, Toan Huynh, Feng Shen, Wenbin Du, and Rustem F. Ismagilov, "Theoretical Design and Analysis of Multivolume Digital Assays with Wide Dynamic Range Validated Experimentally with Microfluidic Digital PCR," Analytical Chemistry 2011 83: 8158-8168.

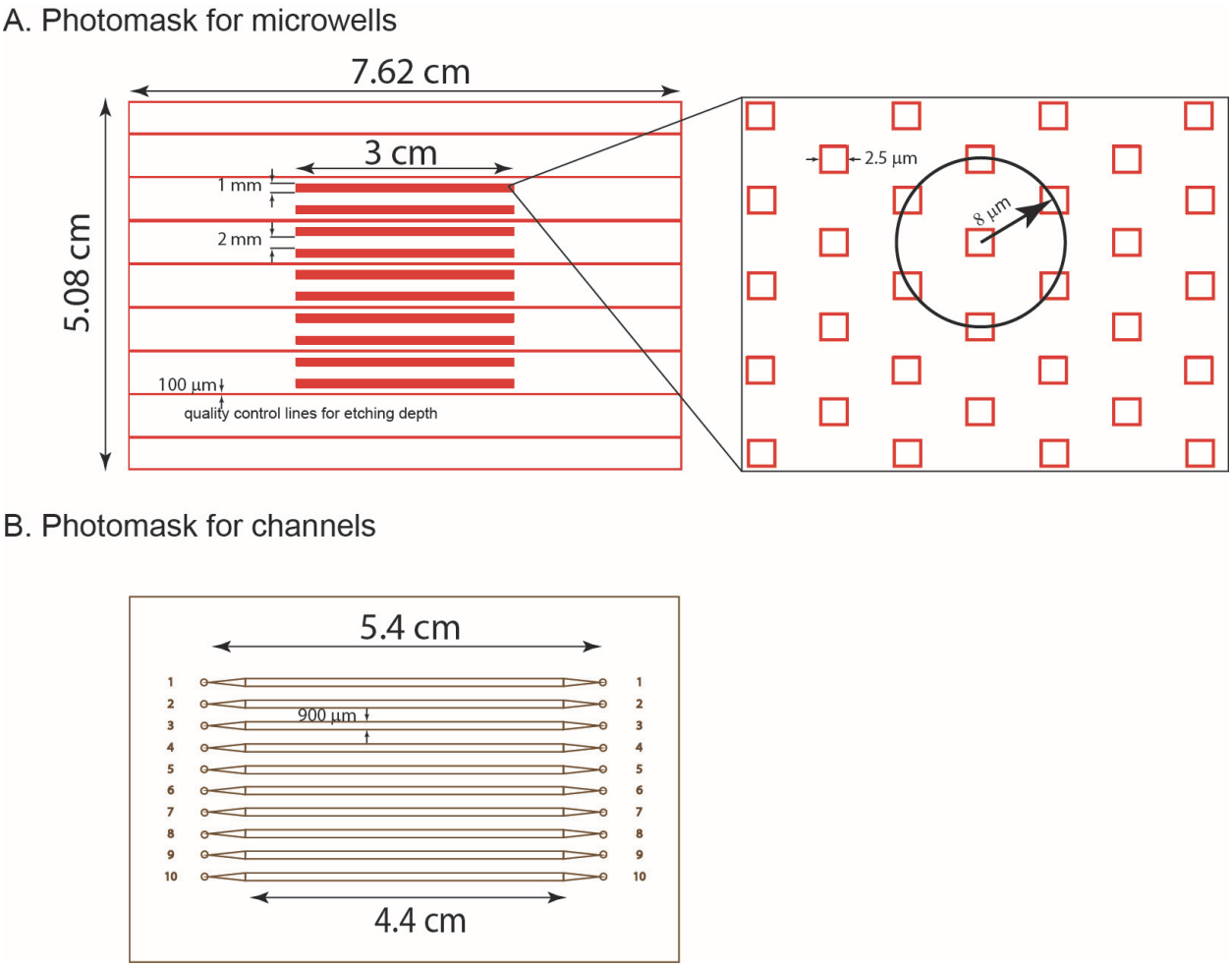

Figure S1. Photomask design. (A) Each channel contains a total of 541,250 microwells (125 vertical x 4330 horizontal), arranged in a hexagonal pattern with a center-to-center spacing of 8 µm. Channels were divided into 22 regions, each of which consisted of 24,604 microwells. Horizontal stripes with a width of 100 µm were included to control the etching depth and uniformity across the chip. (B) Channels were arranged to precisely match the microwell features. An etching depth of 50 µm by isotropic HF etching yields an actual channel width of 1,000 µm."

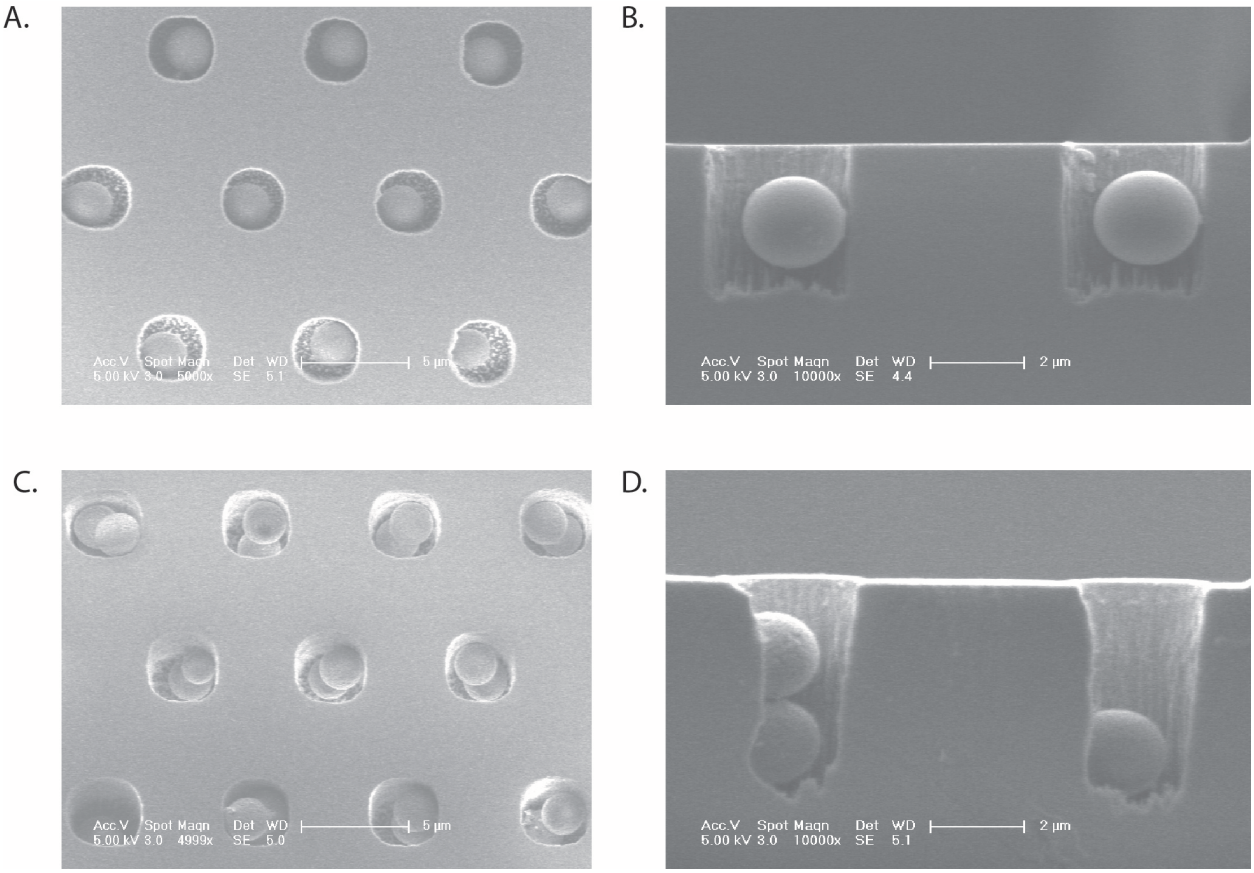

Figure S2. Etching profile examined by SEM. Etching depth needs to be precisely controlled to confine single beads (A and B). The dimension for the etched microwells is approximately 3 µm in diameter and 3 µm in depth, just enough to accommodate a single 2.7 µm bead. Over-etched microwells (C and D) can load more than one bead and thus were not used in the experiment.

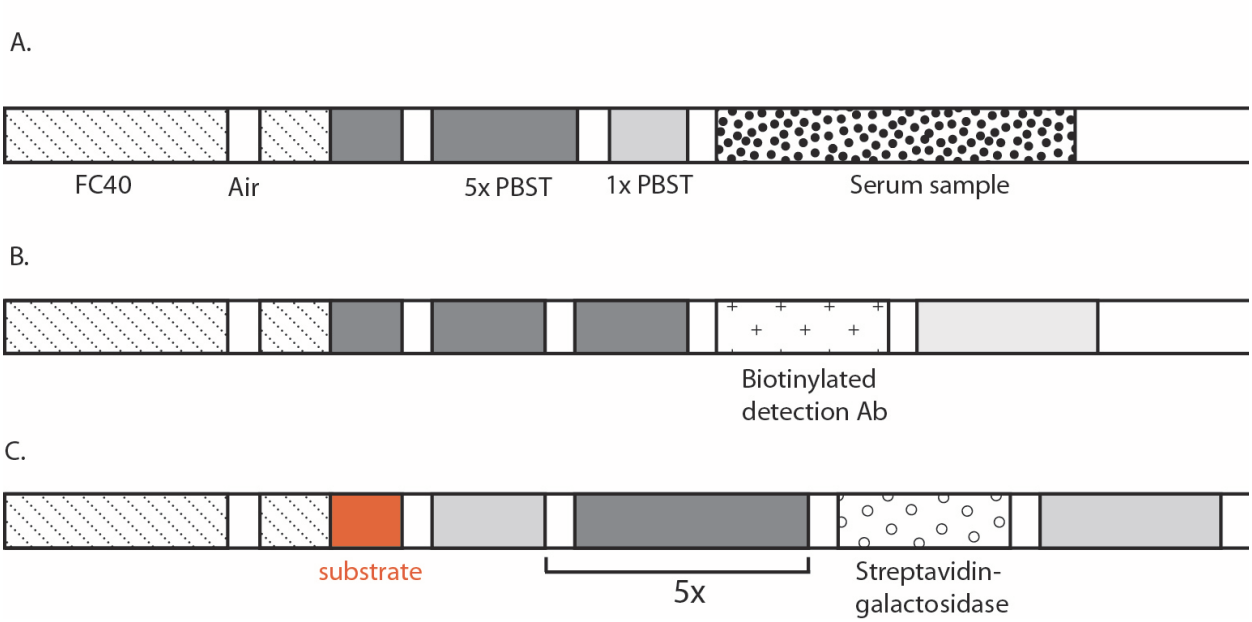

Figure S3. Solution sequences used for on-chip immunoassays. Solutions were loaded in Teflon tubing with air spacers and infused into channels using a syringe pump at a controlled flow rate. See experimental section for solution volumes.

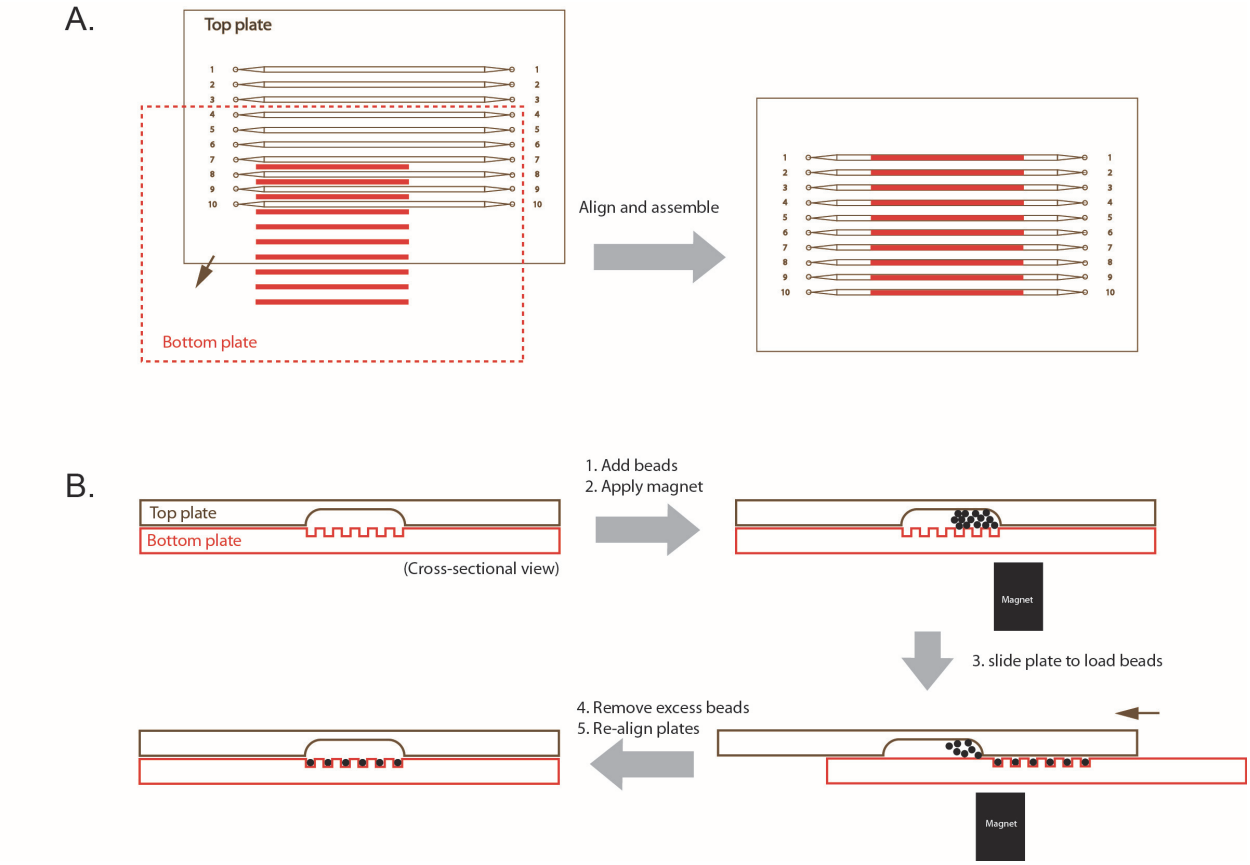

Figure S4. Device assembly and operation to perform the on-chip digital assay. (A) Two complementary microfluidic plates were assembled and aligned with the etched features facing each other. (B) The bead slurry was injected into the channels and then loaded into the microwells using a magnet and a slipping motion. Excess beads were removed and the plates were realigned.

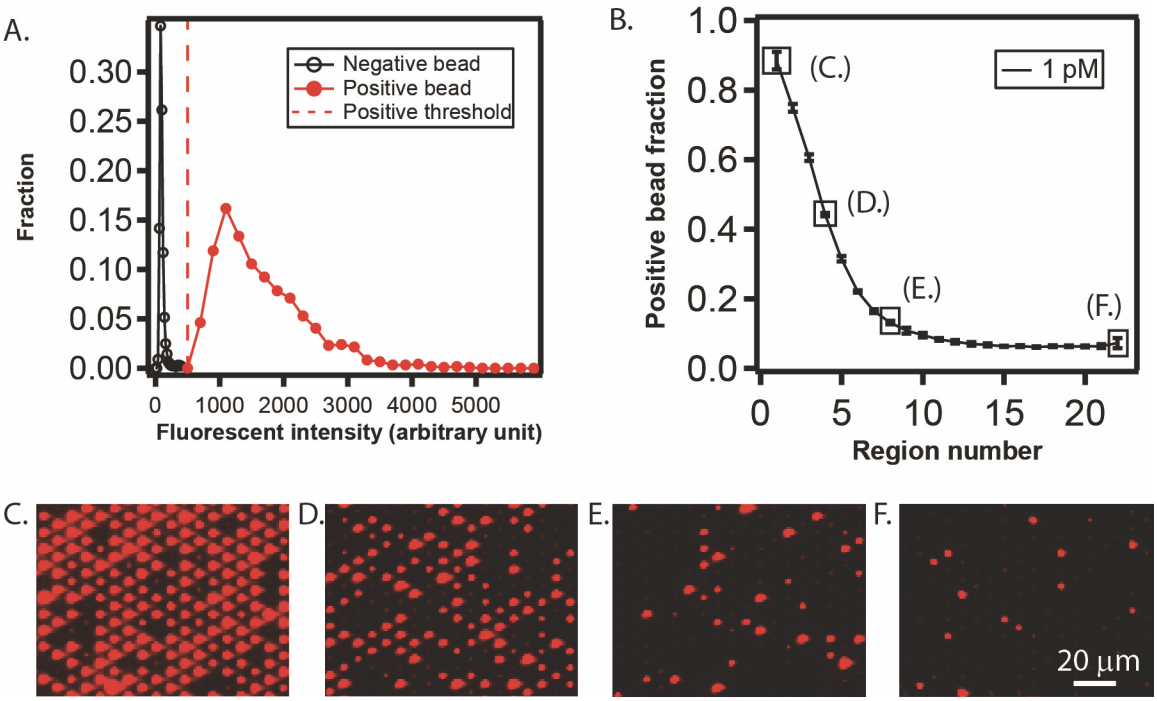

Figure S5. Experimental results and analysis. (A) Histogram of average fluorescence intensity for negative and positive bead fractions. Fluorescence signals ("positive" beads) that arise from enzymatic activities are clearly differentiated from the background fluorescence signal ("negative" beads) and provides the justification of a fluorescence intensity threshold of 500 a.u. (red dashed line). (B-F) Characteristic readouts acquired at different positions (region numbers) along the channel for the 1.0 pM curve from Figure 4.

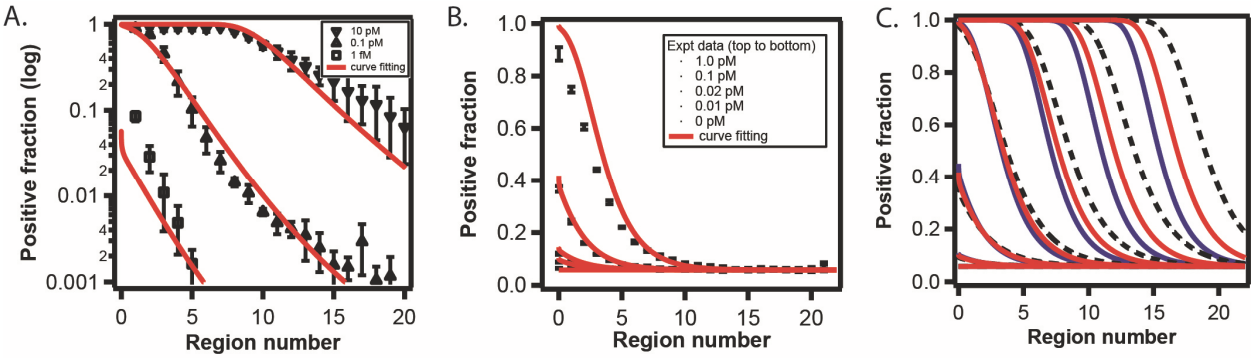

Figure S6. (A) Curves of best fit for Figure 3. The surface concentration of the captured enzyme molecules was simulated using COMSOL Multiphysics, based on a transport-and-adsorption model. A 2D channel was built and meshed with a height of 50 μm and a length of 4 cm. The surface concentration of the capture agent was 1.4 x 10^{-9} mol/m^2; the diffusion coefficient was 0.25 x 10^{-10} m^2/s; the flow velocity was 17 μm/s; and the reaction time was 3600 seconds. The k_{on} for a mono-biotin-labeled enzyme and the streptavidin coated on beads was assumed to be 1.6 x 10^5 M^{-1} s^{-1}; and it was assumed that the total k_{on} is proportional to the number of biotin labeled to the enzyme, which follows a Poisson distribution with an average labeling ratio of 7.9. The k_{off} was assumed to be 5 x 10^{-9} s^{-1}. The surface concentration of the captured enzyme molecules was converted to positive fraction of beads assuming 625,000 beads were loaded. (B) Curves of best fit for the data in Figure 4. Simulation for the concentration of the target molecules was performed similarly as above, with parameters as follows: channel height was 50 μm; channel length was 3 cm; surface concentration of capture antibody was 3.75 x 10^{-9} mol/m^2; k_{on} was 2 x 10^5 M^{-1} s^{-1}; k_{off} was 8 x 10^{-7} s^{-1}; the diffusion coefficient was 0.9 x 10^{-10} m^2/s; flow velocity was 33 μm/s; and reaction time was 4800 seconds. The surface concentration of the captured target molecules was multiplied by a labeling efficiency of 4%, converted to a positive fraction of beads assuming 540,000 beads, then added to the experimental measured background of 0.06 (positive fraction of beads). Given the complexity in the experiment including the matrix effect in the serum, heterogeneous activities of molecules, and non-specific binding, the theoretical fit to experimental data ranging from 0 pm to 1.0 pM was acceptable and as expected the fits deviate from experimental data for the high concentration range (>1.0 pM, not shown) and the origin of the deviation will be a subject for future investigation. (C) Impact of drift velocity, and thus capture efficiency, on assay performance. The concentration series from bottom to top is 0 pM, 0.01 pM, 0.1 pM, 1 pM, 10 pM, 100 pM and 1000 pM. For each concentration condition, three drift velocities were simulated, represented by the blue (30 μm/s for 5400 s), red (as in B, 33 μm/s for 4800 s), and dashed lines (38 μm/s for 4200 s). The impact of the drift velocity on the position of the curves, thus the spatial distribution of the trapped analytes along the channel, is more substantial for the high concentration conditions. As a result, the drift velocity will have a more pronounced effect on the dynamic range of the assay than the sensitivity.